Hindawi
Scientific Programming
Volume 2022, Article ID 9616454, 10 pages
https://doi.org/10.1155/2022/9616454

Research Article

Design and Numerical Simulation of an Odometer Wheel Used in an Ultrasonic In-Line Inspection Tool

Liangxue Cai,[1,2,3] **Liang Guan**,[1] **Xu Qin**,[1] **Lipeng Chen**,[1] **and Guangli Xu**[1,3]

[1]*School of Oil & Natural Gas Engineering, Southwest Petroleum University, Chengdu, China*
[2]*Shandong Key Laboratory of Oil & Gas Storage and Transportation Safety, Qingdao, China*
[3]*Oil & Gas Fire Protection Key Laboratory of Sichuan Province, Chengdu, China*

Correspondence should be addressed to Liangxue Cai; cailiangxue-184@163.com and Guangli Xu; 530xugl@163.com

Received 1 May 2022; Accepted 11 June 2022; Published 28 June 2022

Academic Editor: Xiaofeng Xu

An odometer wheel is used to measure forward distance for a piezoelectric ultrasonic device, and it plays a key role in locating defections. Buckling and skidding are its main problems in applications. Based on a self-developed in-line inspection tool, an odometer wheel was designed according to mechanical design principles. A finite element model on scale of 1 : 1 was built to simulate mechanical performance of the odometer wheel. Results show that the maximum Mises stress under the worst condition is far less than the elastic limit of chosen stainless steel, and deformations of swing arms are slight. Acting forces under different conditions also meet requirements of antiskid. It indicates that the designed object has good performance in terms of structure stability and skid prevention.

1. Introduction

Along with the rapid development of oil and gas pipeline network in China, upgrading from digitization to intelligentization is an apparent trend in pipeline constructions and managements [1]. Nondestructive testing (NDT) can supply pipe's basic data, and it plays an important role in developing intelligent pipelines. The ultrasonic in-line inspection technology is an efficient way to detect cracks [2] which appear and grow in pipes exposed to various environmental media [3] and loading conditions [4]. Several types of ultrasonic inspection tools are in progress of developing. A typical piezoelectric ultrasonic device usually contains ultrasonic probe array, data acquisition system (DAS), odometer wheel, driving cups, and battery [5]. An odometer wheel is used to locate flaws during in-line inspection [6], and it plays an important role in processing inspection data [7]. Structural stability and skid prevention are essential factors to guarantee an odometer wheel's normal performance, and hence they should be analyzed particularly in designing an odometer wheel.

Zang et al. [8] studied the reason why an internal detector's odometer wheel skids, and they suggested that the diameter of an odometer wheel should be as small as possible on the premise that an odometer wheel meets other requirements. Li et al. [9] analyzed the kinematics of an odometer wheel through numerical simulation. It is found that the odometer wheel causes a larger odometer error when the speed of its roller's rotation speed is higher when it passes through a girth weld. Xie et al. [10] investigated the preprocessing algorithm of odometer wheel positioning data, and they proposed a preprocessing algorithm for in-line detector odometer wheel positioning data based on the Kalman filter. The accuracy of locating a detector was improved effectively [11]. The abovementioned studies mainly focus on improving the performance of an odometer wheel's locating function, while the structural stability of an odometer wheel as well as its antiskid performance [12] is not analyzed considering extreme conditions during in-line inspection [13].

Based on parameters of a self-developed piezoelectric ultrasonic device for detecting pipes with diameter of 219 mm, an overall structure of a relative odometer wheel was designed according to mechanical design principles and actual application conditions. A finite element model was built using ANSYS to analyze its structural stability under

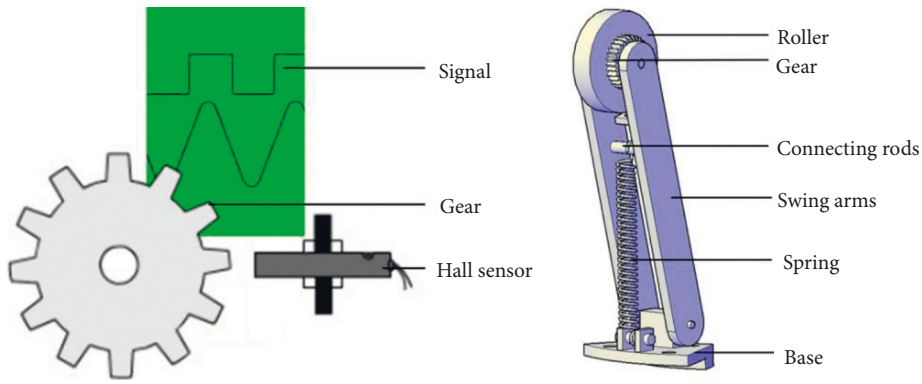

Figure 1: Structure of an odometer wheel.

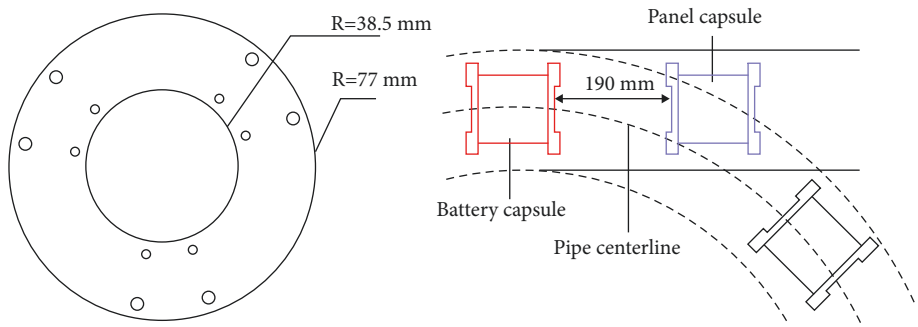

Figure 2: Structure of a battery capsule's end.

four kinds of application conditions. Acting forces on a pipe's inner wall by the roller were discussed to check its antiskid performance.

2. Structural Design of an Odometer Wheel

An ultrasonic in-line inspection tool is pushed forward by pressure difference between its front and back in oil and gas pipes. As a spring is used in an odometer wheel, it pulls the swing arm outward so that a roller installed at an end of the swing arm can press tightly against the inner wall of a pipe. A gear that rotates synchronously is set on one side of the roller, and a Hall sensor is used to capture the rotation signal of a gear [14], as shown in Figure 1. After the signal being processed and stored, it is converted into a required odometer signal, and finally we can get the locating data.

A typical odometer wheel mainly contains swing arm, roller, gear, mounting base, spring, sensor, connecting rods, etc. [15]. No buckling of an odometer wheel and roller skidding on the inner wall of a pipe is the premise of an odometer wheel's good performance [16]. The self-developed piezoelectric ultrasonic device size is available for pipes $\Phi 219 \times 7.5$ mm, and its minimum pipeline bend radius is $3D \times 90^{\circ}$. An odometer wheel is placed at the end of a battery capsule, and Figure 2 shows its structure and sizes. The mounting base is connected with battery capsule's end face and an annular plate fixing a driving cup. In constructing projects of oil and gas pipelines, the usual minimum radius of pipelines is recommended as 5D [17], and it should not be less than 4D [18], which are 1095 mm and 876 mm for 219 mm pipes, respectively.

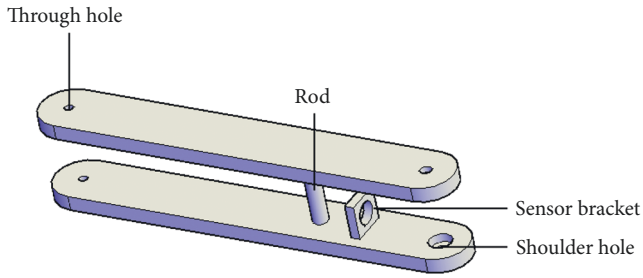

Figure 3: Structure of swing arms.

2.1. Swing Arm. A Swing arm is designed to keep tight contact between a roller and a pipe's inner wall during in-line inspection. It is a pendulum component and can be damaged with high probability in applications. In order to enhance the reliability, a kind of double swing arms structure is adopted to improve its stability in design (Figure 3). Structures of two swing arms are same, and they are set symmetrically. Two rods located at one end and middle part of arms are used to connect these two arms. The latter rod serves as a fulcrum for the spring as well. An axle is set at one end to support the roller and gear.

The free space between two adjacent capsules and extreme conditions in-situ applications of an in-line inspection tool are key factors to determine the length of swing arms.

For the piezoelectric ultrasonic device, the free space's axial length is 190 mm and the extreme loading condition occurs when it passes through an outer side accompanied with a dent (depth 6 mm) of a 3D elbow. Besides, stricter performance is required for a spring when the length of a swing arm decreases. Hence, the length of swing arms was designed as 150 mm. Considering requirements of strength and stiffness, the width and thickness of a swing arm were set as 20 mm and 5 mm, respectively. Detailed strength and stability analysis were conducted by numerical simulation in following contents.

In view of swing arms' smooth rotation, the end of a swing arm jointed with a mounting base was set as a circular arc with diameter of 20 mm. The structure of another end was same. A through hole and a shoulder hole were perforated at centers of the above two arcs, respectively. A bracket was welded on a swing arm to fix a Hall sensor. The sensor probe faces the gear side to capture rotation signals of a roller.

2.2. Roller and Gear. The function of a roller and gear is to measure forward distances of an inspection device using a periodic pulse signal generated by a Hall sensor when a gear rotates. Meanwhile, the signal is also treated as the initial point in DAS to start repetitive detection. When a detector moves forward at a certain velocity, small diameter of a roller leads to high rotation speed. Consequently, possibility of a roller's abrasion and skid rises rapidly. In addition, considering that the axial resolution of self-developed piezoelectric ultrasonic device is 5 mm and the free space between two adjacent capsules, the roller's diameter is determined as 47.75 mm. The number of a gear's teeth (n) can be calculated by

$$n = \frac{\pi D}{A}, \tag{1}$$

where D is the diameter of a roller and A is the axial resolution. Then, 30 teeth were obtained for the designed gear. The edge of a gear cannot contact with a pipe's inner wall when a roller rolls forward. Hence, a gear's diameter is required to be less than a roller's diameter. On the other hand, large pitch which leads to big diameter of a gear is needed to guarantee a Hall sensor's normal performance. Therefore, the gear's diameter is determined as 25 mm, as shown in Figure 4.

Skid prevention plays a key role in improving the accuracy of measuring distances [8]. Increasing the contact area and frictional coefficient between a roller and a pipe's inner wall can be considered in design. As the inner diameter of pipe segments used in ultrasonic testing experiments was 204 mm, the cross section of roller's contact surface along radial direction is designed as an arc with radius of 102 mm. Meanwhile, roller's contact surface is knurled.

2.3. Mounting Base. The mounting base in this project functions in three aspects: a bracket to install swing arms, a pivot to fix a spring, and a connector to fasten the odometer wheel on the battery capsule. Based on the structure of capsule's end shown in Figure 2, a block projected as an annular sector was designed. Its outer radius and inner radius are 77 mm and 38.5 mm, respectively. The bottom is step-shaped to match the structure of capsule's end. The block is fixed on the end face by four bolts, of which two bolts are connected to the annular plate and other bolts to the end of capsule. The built mounting base is shown in Figure 5.

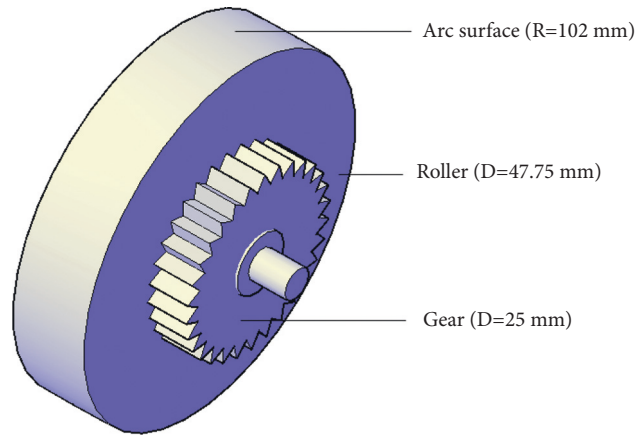

Figure 4: Structure of a roller and gear.

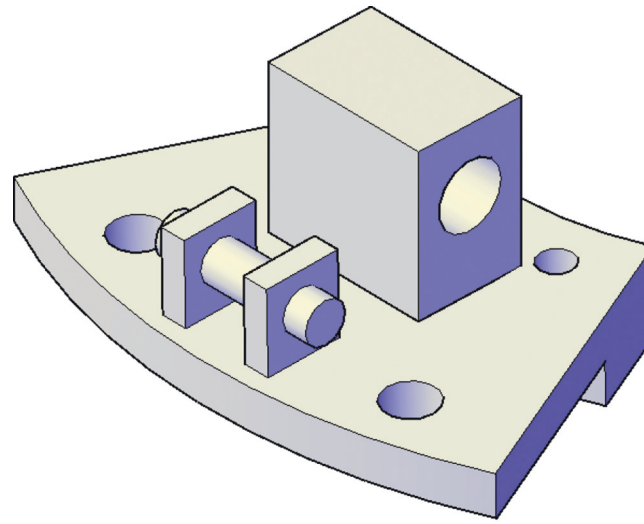

Figure 5: Structure of a mounting base.

2.4. Spring. When a detector moves forward in a pipe, the acting force between the roller and the inner wall is determined by a spring. A steady acting force with a suitable value can enhance the ability of skid prevention. During in-line inspection using the piezoelectric ultrasonic device, the spring acts under three typical conditions, i.e., the odometer wheel passes through (1) an inner side of a 3D elbow, (2) straight pipe, and (3) an outer side accompanied with a dent (depth 6 mm) of a 3D elbow, as shown in Figure 6. The minimum and maximum lengths of the spring occur in conditions (1) and (3) are 77 mm and 82 mm, respectively. In a certain condition, the minimum spring force applied on the odometer wheel is determined by free length and spring rate while the spring force's variation is determined by

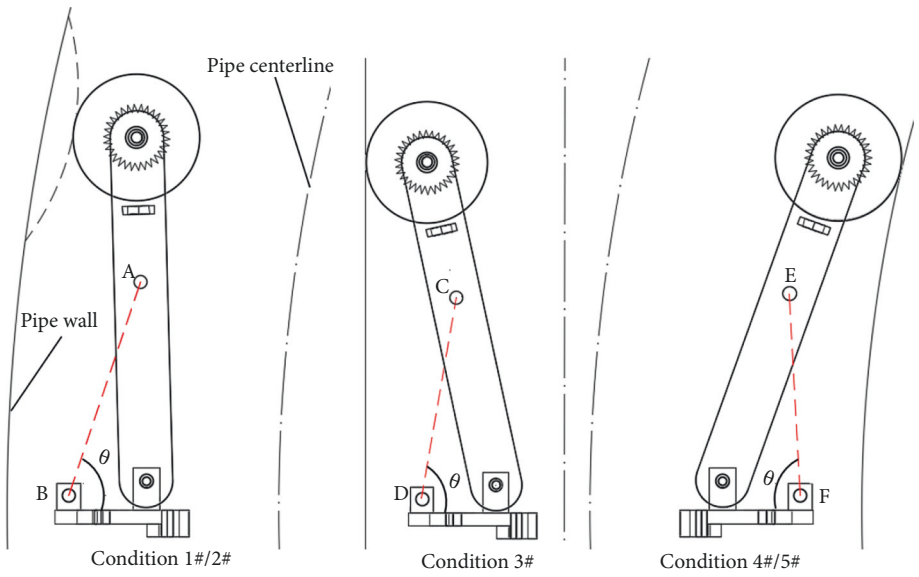

Figure 6: Sketch of typical conditions passed by an odometer wheel.

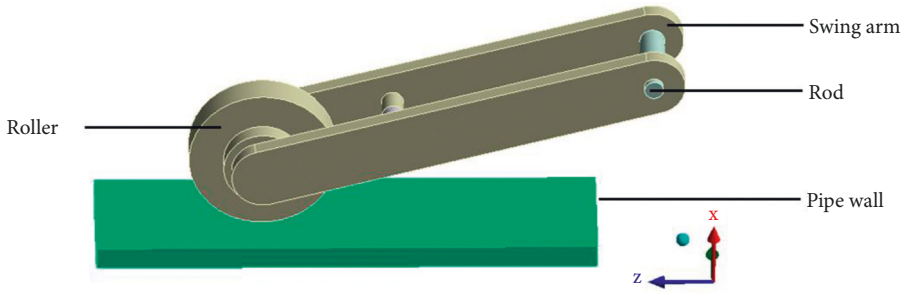

Figure 7: Physical model of the odometer wheel.

spring rate. Hence, four kinds of spring were compared with free length and spring rate of (1) 62 mm and 8 N/mm, (2) 65 mm and 10 N/mm, (3) 67 mm and 12 N/mm, and (4) 69 mm and 15 N/mm, respectively. The minimum spring force is set as 120 N in design and the above four springs meet this requirement.

3. Finite Element Model of the Odometer Wheel

Analyzing structure stability and skid prevention of the designed odometer wheel is necessary for its good performance. Maximum stress and deformation under extreme loading conditions are key criteria for structure stability while acting force between a roller and pipe's inner wall under extreme conditions is a critical factor in assessing skid prevention. The finite element software ANSYS is powerful and convenient to conduct mechanical simulation of this object with complex structure.

3.1. Physical Model. Based on the designed odometer wheel, a physical model on the scale of 1 : 1 is built as shown in Figure 7. As mounting base, Hall sensor and its bracket, gear have little affections on the odometer wheel's mechanical characteristics, the following simplifications are assumed: (1) the rod connecting swing arms and mounting base is treated as a fulcrum and mounting base was ignored, (2) Hall sensor and its bracket were ignored, and (3) the gear was simplified as a cylinder with diameter equal to the diameter of its point circle. The spring was replaced by an equivalent pull force. A pipe wall with axial length of 160 mm, circumferential length of 40 mm, and thickness of 7.5 mm was used. The values of structure's sizes are listed in Table 1.

Table 1: Parameters of physical model for the odometer wheel (units: mm).

Components	Parameters	Values
Swing arms	Length	150
	Width	20
	Thickness	5
	Arc's diameter	20
Roller	Diameter	47.75
	Thickness	10
	Contact surface's radius	102
Gear	Diameter	25
	Thickness	6
Pipe wall	Axial length	160
	Circumferential length	40
	Thickness	7.5

Table 2: Input parameters of material properties.

Components	Mark	Yield Strength/MPa	Tangent modulus (MPa)	Elastic modulus (GPa)	Poisson ratio
Pipe wall	L245	245	777	203	0.3*
Odometer wheel	06Cr19Ni10	220	752	193	0.3*
	2014-T4	230	1429	71	0.3

*Value of Poisson ratio is referred to data given by Su et al. [22].

3.2. Material Properties. The object in simulation is made of steel. The metal has an initial elastic region in which deformation is proportional to the load, while an irrecoverable plastic strain occurs when stress exceeds elastic limit. In order to simulate the mechanical behaviour of steel accurately during operation of the odometer wheel, the bilinear isotropic hardening model was used to describe the material's stress-strain curve. In this model, the curve's initial slope is elastic modulus of the steel. Beyond the yield stress, the plastic strain develops and the stress and strain continue along a line with a slope equal to tangent modulus.

Steel pipe L245 [19] was used in ultrasonic testing experiments. There are two options for the material of the mileage wheel: stainless steel 06Cr19Ni10 [20] and 2014-T4 aluminum alloy [21]. Initial parameters for these three materials used in bilinear isotropic hardening model were calculated according to their properties, and relative values used in simulations are listed in Table 2.

3.3. Meshing. Meshing is the basis of finite element analysis, replacing the original continuum with a collection of finite elements. Element SOLID186 was used to simulate the steel. An accurate calculation can be got by meshing densely. In view of the odometer wheel is a main object in simulation analysis, its size of meshing is set to overall meshing size. Adopting the Hex Dominant method to mesh is beneficial to keep the grid's regularity for the physical model. Therefore, the overall meshing size was set to 2 mm, and the Hex Dominant method was adopted to mesh. The result of meshing was 72821 nodes and 17319 elements, as shown in Figure 8.

3.4. Boundary Conditions and Loads. There are two contact interactions in simulation, i.e., interaction between the roller and pipe wall and that between swing arms and the rod connected to mounting base. Both problems are flexible-to-flexible contact. Contact unit CONTA174 and target unit TARGE170 were chosen to form surface-to-surface three dimensional contact pairs. The Lagrange frictional contact logic of face to face was defined in contact interactions, and the contact behavior was set asymmetrically. The pipe inner wall and the through hole's wall in swing arms were set as the target surface. Rolling surface of the roller and side face of the rod were set as the contact surface.

A pipe is immobile during in-line inspection and fixed constraints were applied to the pipe's outer surface to make the model's boundary closer to actual operating environments. As the rod installed in the mounting base cannot rotate, full constraints were applied to the side face of the rod.

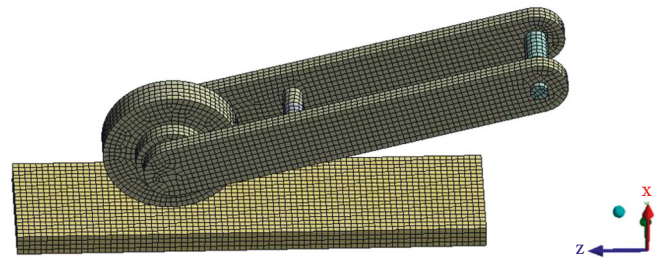

Figure 8: Odometer wheel meshing.

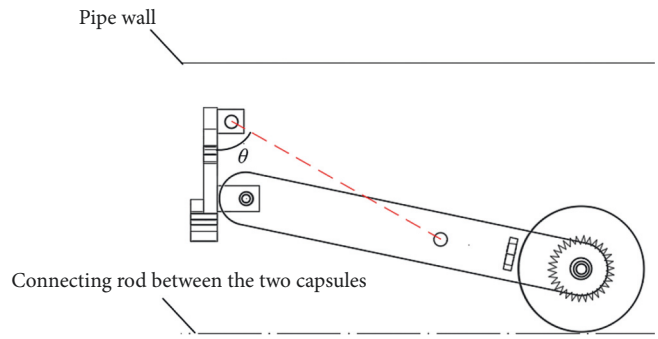

Figure 9: The extreme condition.

The profile of oil and gas pipeline is determined by terrain, and there usually are a large amount of elbows. The recommended minimum radius of pipelines is 4D [18] while the piezoelectric ultrasonic device size is available for 3D. Moreover, there are various kinds of defections existing in oil and gas pipelines and dents have the greatest influence on the operating performance of an odometer wheel. As the diameter of pipe segments used in ultrasonic testing experiments is less than 300 mm, the maximum depth of dents allowable in projects is 6 mm [23]. In order to assess the designed odometer wheel's performance, five typical conditions and an extreme condition were taken into account in numerical analysis. The typical conditions include passing through outer side of a 3D/4D elbow with a 6 mm dent, straight pipe, and inner side of a 3D/4D elbow as shown in Figure 6. Besides, the extreme loading condition for the odometer wheel is that the roller and connecting rod between a battery capsule and a panel capsule are coincident, as shown in Figure 9. The spring's pull force under a certain condition was calculated theoretically and was applied to the rod located at the middle part of swing arms directly. Initial pull forces used in simulations are listed in Table 3, where the

Table 3: Input values of initial loads.

Conditions	Outer side with a 6 mm dent		Straight pipe	Inner side		Extreme condition
	3D	4D		3D	4D	
Serial number	1#	2#	3#	4#	5#	6#
1# spring's pull force (F/N)	152	144	136	120	128	232
2# spring's pull force (F/N)	160	150	140	120	130	260
3# spring's pull force (F/N)	168	156	144	120	132	288
4# spring's pull force (F/N)	180	165	150	120	135	330
Pull force's direction (θ/°)	76	76	80	82	81	61

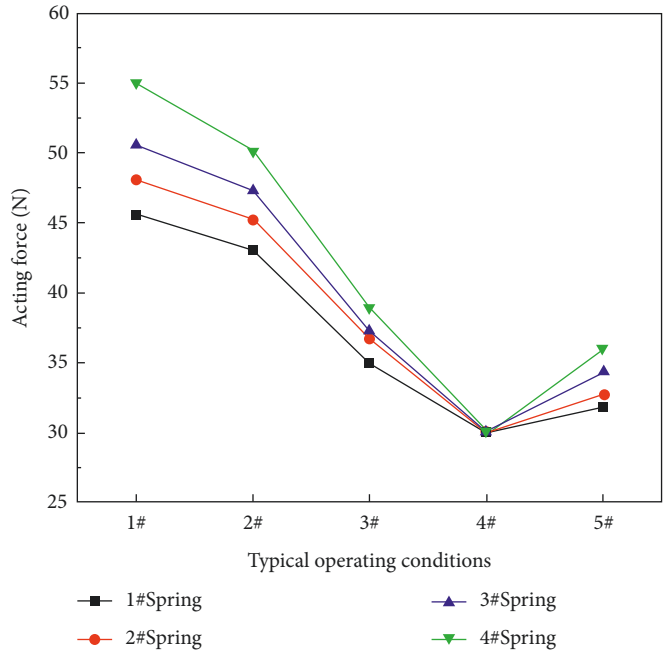

Figure 10: Acting forces under different conditions.

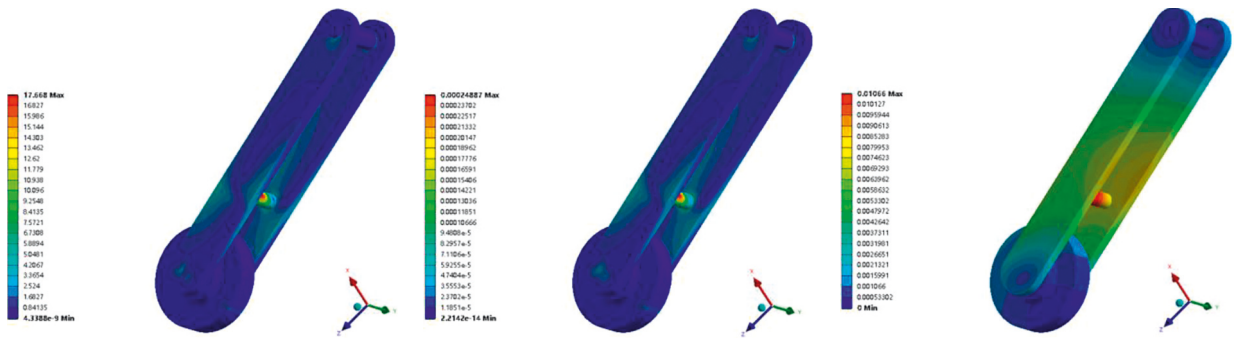

(a) (b) (c)

Figure 11: Mises stress, strain, and deformation cloud diagram of 2014-T4 aluminum alloy (1#).

pull force direction which is the angle between center axis of spring and mounting base surface is denoted as θ.

4. Analysis of Simulation Results

4.1. Antiskid Performance Analysis. Low stiffness coefficient of a spring, powdery dirt in pipelines, nonuniform velocity of a detector can lead to skid problem of an odometer wheel. The essential reason is low frictional coefficient and acting force between a roller and pipe's inner wall. The roller's contact surface is knurled to increase frictional coefficient. The dynamic characteristics of acting force under different conditions with different springs are presented in Figure 10. A suitable spring should meet two principles, i.e., the acting

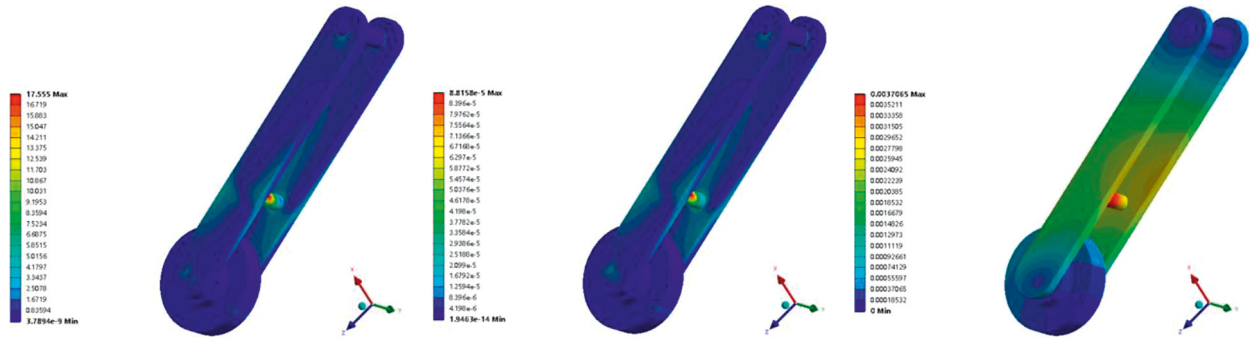

(a) (b) (c)

Figure 12: Mises stress, strain, and deformation cloud diagram of 06Cr19Ni10 (1#).

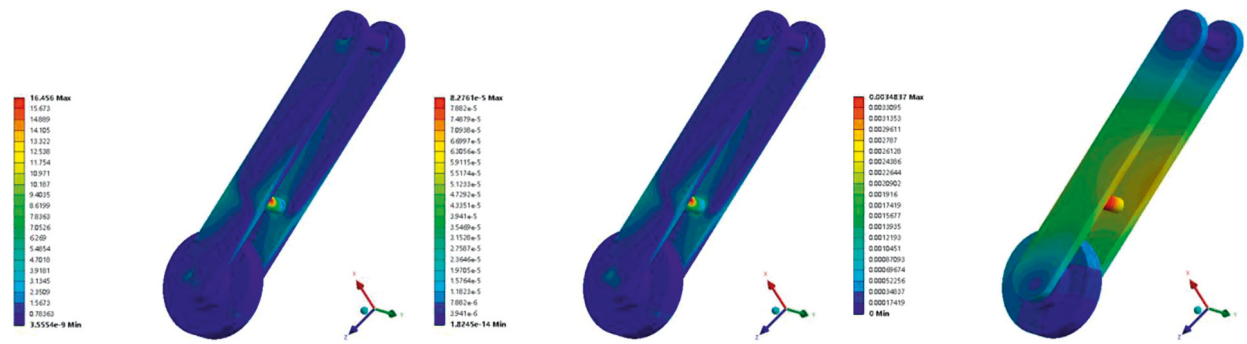

(a) (b) (c)

Figure 13: Mises stress, deformation, and strain cloud diagram (2#).

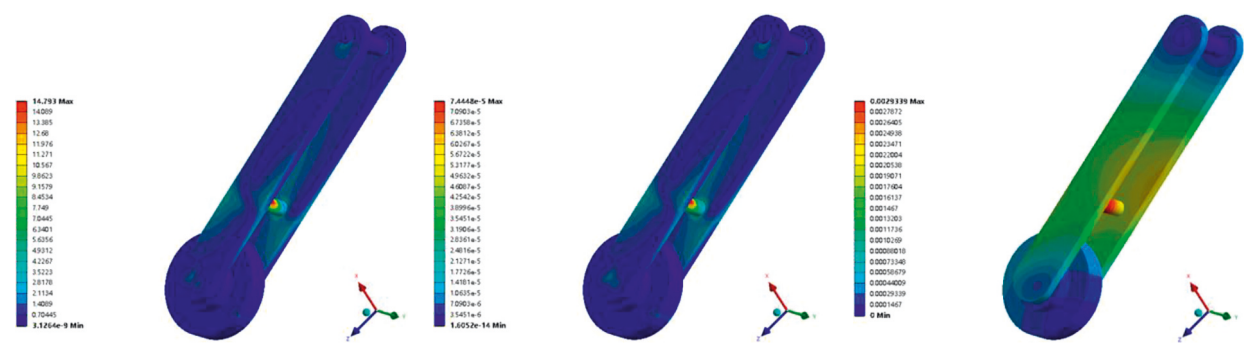

(a) (b) (c)

Figure 14: Mises stress, deformation, and strain cloud diagram (3#).

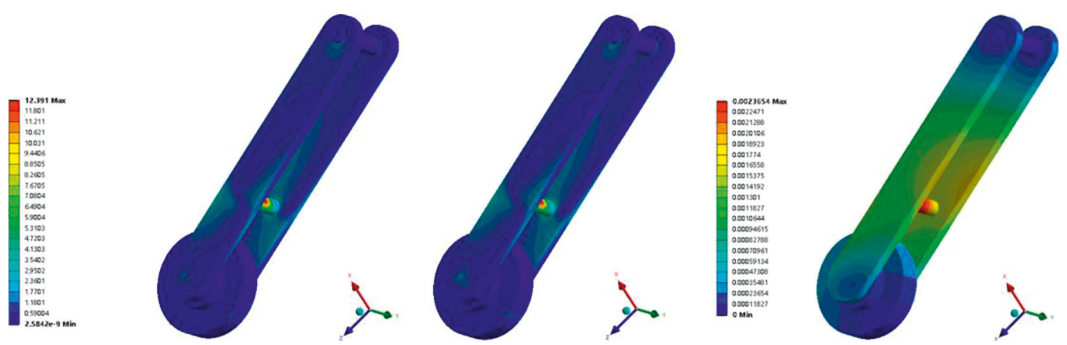

(a) (b) (c)

Figure 15: Mises stress, deformation, and strain cloud diagram (4#).

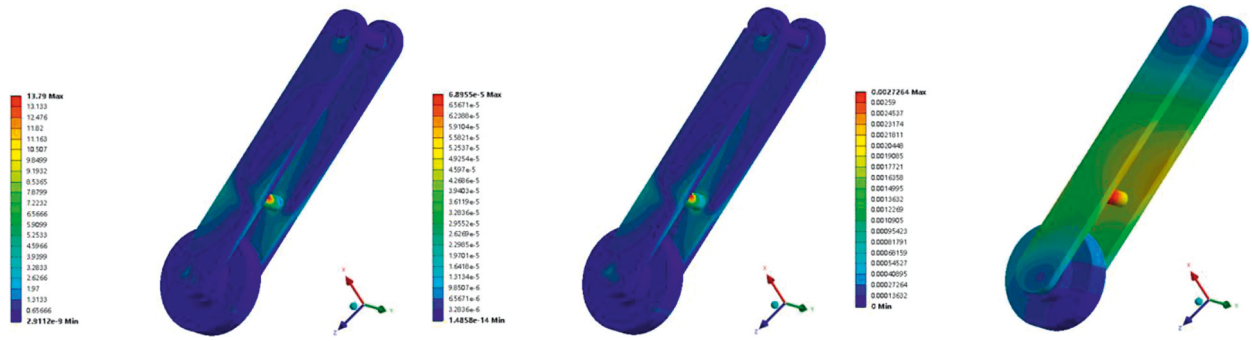

(a) (b) (c)

Figure 16: Mises stress, deformation, and strain cloud diagram (5#).

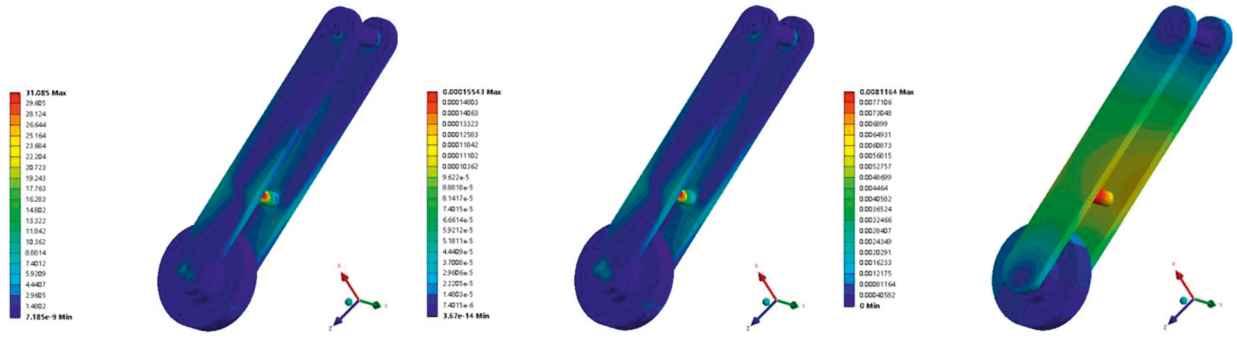

(a) (b) (c)

Figure 17: Mises stress, deformation, and strain cloud diagram (6#).

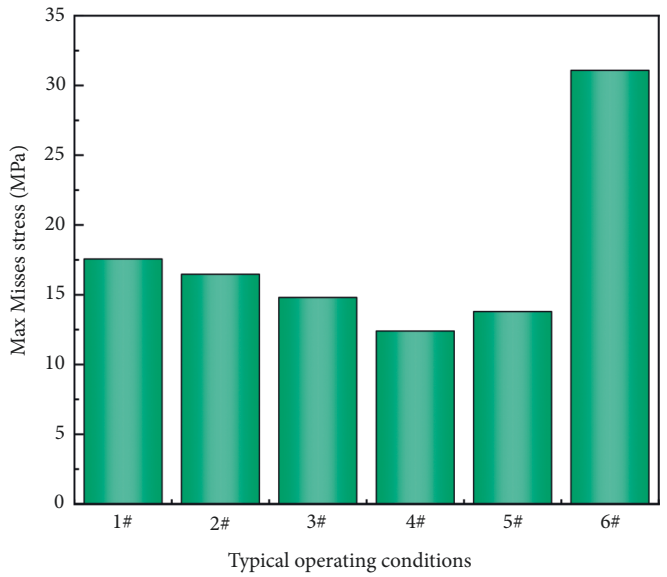

Figure 18: Maximum Mises stresses in six conditions.

force meets requirements for antiskid and its variation under various working conditions is small. The variation of 3# spring and 4# spring is relatively large, and the difference between maximum value and minimum value exceeds 50% of the minimum value. Although 1# spring has a small change in various typical operating conditions, the acting force under 1# working condition is only 45 N. Hence, 2# spring was chosen in design. The maximum value of acting

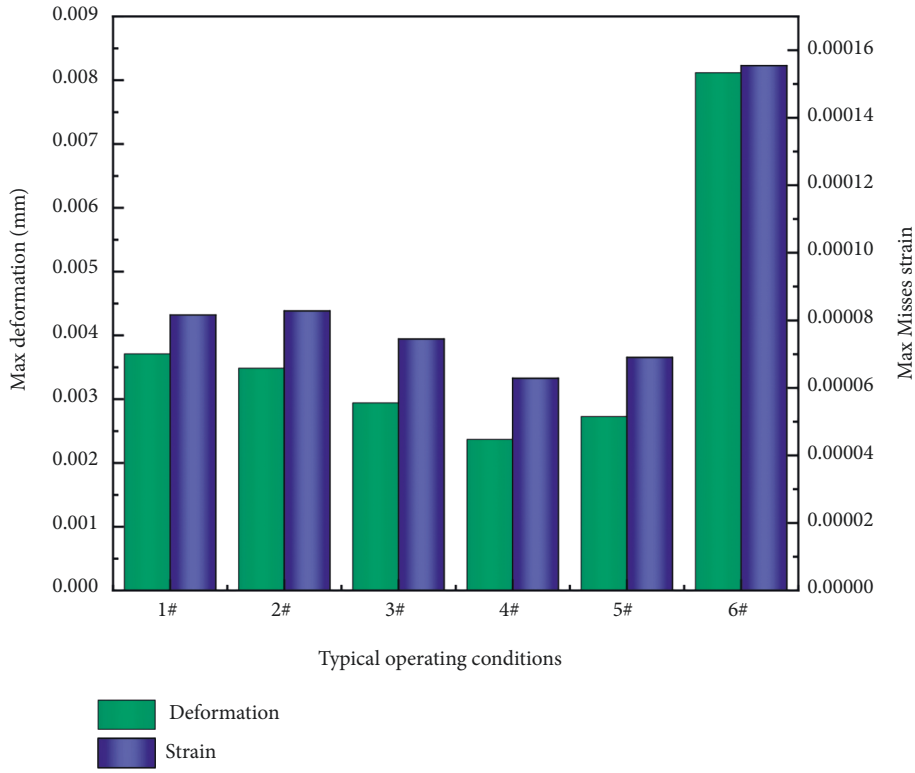

Figure 19: Maximum Mises strain and deformations in six conditions.

force is 48.08 N, and the minimum value is 30.03 N in five working conditions. It indicates that the design odometer wheel meets requirements of antiskid.

4.2. Material of Odometer Wheel Analysis. In order to determine the appropriate material, odometer wheels made of stainless steel 06Cr19Ni10 and 2014-T4 aluminum alloy were simulated and analyzed in five working conditions and the extreme condition. Taking the 1# working condition as an example, as shown in Figures 11 and 12, the Mises stress of all working conditions of the two materials are similar. The strain and deformation of aluminum alloy are larger than those of stainless steel. Considering the self-developed piezoelectric ultrasonic device was made of stainless steel, stainless steel 06Cr19Ni10 is selected in order to keep the uniformity and stability of a device's material.

4.3. Structural Stability Analysis. Figures 13 and 14 present the Mises stress, strain, and deformation. Figure 15 shows the cloud diagrams of the odometer wheel in all conditions. In all working conditions, maximum values of Mises stress (Figure 16), Mises strain (Figure 17), and total deformation occur at the rod in middle part of swing arms, which are compared in Figures 18 and 19. Corresponding values for condition 1# with the worst mechanical state and extreme condition 6# are (17.55 MPa, 0.0000882, 0.00371 mm), (31.09 MPa, 0.000155, 0.00812 mm), respectively. Results show that maximum Mises stresses in condition 1# and condition 6# are far less than the elastic limit of stainless steel 220 MPa. The deformation in extreme condition has little influence on the odometer wheel's normal performance, and it can be ignored. It indicates that the designed odometer wheel has good performance in term of structure stability.

5. Conclusion

The piezoelectric ultrasonic in-line inspection technology is an effective way to conduct detection of oil and gas pipelines. Based on a self-developed piezoelectric ultrasonic device, mechanical design principles were discussed and an odometer wheel was designed. The material of odometer was chosen stainless steel 06Cr19Ni10. The free length of spring and spring rate were chosen 65 mm and 10 N/mm. Five typical conditions under which the odometer wheel works were summarized according to in-situ applications. A finite element model was built by the software ANSYS, and the mechanical performance of the odometer wheel were analyzed. The maximum Mises stress (31.09 MPa) under extreme condition 6# is far less than the elastic limit (220 MPa) of chosen stainless steel. Maximum deformation and Mises strain of the odometer wheel are 0.00812 mm and 0.000155. Good performance of structure stability is shown for the designed odometer wheel. The acting force under five working conditions varies from 30.03 N to 48.08 N. The designed object also meets requirements of antiskid.

Data Availability

The data used to support the findings of this study are included within the article.

Conflicts of Interest

The authors declare that they have no conflicts of interest.

Acknowledgments

This work was financially supported by Fundamental Research Funds for the Central Universities (19CX05007A) and the National Natural Science Foundation of China (No. 51606160).

References

[1] J. J. Zhang, H. Su, and P. Gao, "Resilience-based supply assurance of natural gas pipeline networks and its research prospects," *Acta Petrolei Sinica*, vol. 41, no. 12, pp. 1665–1678, 2020.

[2] O. Taylan, M. A. Sattari, I. Elhachfi Essoussi, and E. Nazemi, "Frequency domain feature extraction investigation to increase the accuracy of an intelligent non-destructive system for volume fraction and regime determination of gas-water-oil three-phase flows," *Mathematics*, vol. 9, no. 17, Article ID 2091, 2021.

[3] H. Zhang, S. Dong, J. Ling, L. Zhang, and B. Cheang, "A modified method for the safety factor parameter: the use of big data to improve petroleum pipeline reliability assessment," *Reliability Engineering & System Safety*, vol. 198, Article ID 106892, 2020.

[4] O. Taylan, M. Abusurrah, S. Amiri, E. Nazemi, E. Eftekhari-Zadeh, and G. H. Roshani, "Proposing an intelligent dual-energy radiation-based system for metering scale layer thickness in oil pipelines containing an annular regime of three-phase flow," *Mathematics*, vol. 9, no. 19, Article ID 2391, 2021.

[5] M. S. Chowdhury and M. F. Abdel-Hafez, "Pipeline inspection gauge position estimation using inertial measurement unit, odometer, and a set of reference stations," *ASCE-ASME Journal of Risk and Uncertainty in Engineering Systems, Part B: Mechanical Engineering*, vol. 2, no. 2, 2016.

[6] X. Zhu, X. Li, C. Zhao, S. Zhang, and S. Liu, "Dynamic simulation and experimental research on the motion of odometer passing over the weld," *Journal of Natural Gas Science and Engineering*, vol. 30, pp. 205–212, 2016.

[7] D. Zelmati, O. Bouledroua, Z. Hafsi, and M. B. Djukic, "Probabilistic analysis of corroded pipeline under localized corrosion defects based on the intelligent inspection tool," *Engineering Failure Analysis*, vol. 115, Article ID 104683, 2020.

[8] Y. X. Zang, C. Qiu, T. H. Hu, and H. Yang, "Causes of slippage of odometer wheels in pipeline inline detectors," *J. Oil & Gas Storage and Transportation,* vol. 35, no. 3, pp. 306–309, 2016.

[9] X. L. Li, J. Z. Chen, Y. L. Ma, R. X. He, and T. Meng, "ADAMS-Based kinematics analysis of the odometer passing over girth weld," *J. China Petroleum Machinery,* vol. 47, no. 4, pp. 118–123, 2019.

[10] Y. Xie, D. Gu, X. Wang et al., "A smart healthcare knowledge service framework for hierarchical medical treatment system," *Healthcare*, vol. 10, no. 1, p. 32, 2021.

[11] H. Xu, Z. X. Li, Y. Y. Li, and L. H. Gong, "Study on the error analysis of pipeline inspection robot mileage wheel localization," *Advanced Materials Research*, vol. 706-708, pp. 1171–1174, 2013.

[12] X. Wu, S. J. Jin, Y. B. Li, Y. K. Xiao, and H. M. Zhao, "Above-ground marker system of pipeline internal inspection instrument based on geophone array," *Journal of Nanotechnol Precision Engineering*, vol. 8, pp. 553–558, 2010.

[13] Y. Li, S. Liu, D. J. Dorantes-Gonzalez, C. Zhou, and H. Zhu, "A novel above-ground marking approach based on the girth weld impact sound for pipeline defect inspection," *Insight - Non-Destructive Testing and Condition Monitoring*, vol. 56, no. 12, pp. 677–682, 2014.

[14] Z. Wang, J. Tan, and Z. Sun, "Error factor and mathematical model of positioning with odometer wheel," *Advances in Mechanical Engineering*, vol. 7, no. 1, Article ID 305981, 2015.

[15] X. Li, S. Zhang, S. Liu, Q. Jiao, and L. Dai, "An experimental evaluation of the probe dynamics as a probe pig inspects internal convex defects in oil and gas pipelines," *Measurement*, vol. 63, pp. 49–60, 2015.

[16] X. Li, S. Zhang, S. Liu, X. Zhu, and K. Zhang, "Experimental study on the probe dynamic behaviour of feeler pigs in detecting internal corrosion in oil and gas pipelines," *Journal of Natural Gas Science and Engineering*, vol. 26, pp. 229–239, 2015.

[17] GB 50253-2014, *Code for Design of Oil Transportation Pipeline Engineering*, China Planning Press, Beijing, China, 2014.

[18] GB 50369-2014, *Code for Construction and Acceptance of Oil and Gas Long-Distance Transmission Pipeline Engineering*, China Planning Press, Beijing, China, 2014.

[19] Gb/T 9711-2017, *Petroleum and Natural Gas Industries-Steel Pipe for Pipeline Transportation Systems*, China Planning Press, Beijing, China, 2017.

[20] Gb/T 24511-2017, *Stainless Steel and Heat Resisting Steel Plate, Sheet and Strip for Pressure Equipments*, China Planning Press, Beijing, China, 2017.

[21] Gb/T 6892-2015, *Wrought Aluminium and Aluminium Alloys Extruded Profiles for General Engineering*, China Planning Press, Beijing, China, 2012.

[22] Y. Su, J. Li, B. Yu, Y. Zhao, and J. Yao, "Fast and accurate prediction of failure pressure of oil and gas defective pipelines using the deep learning model," *Reliability Engineering & System Safety*, vol. 216, Article ID 108016, 2021.

[23] Gb/T. 50251-2015, *Code for Design of Gas Transmission Pipeline Engineering*, China Planning Press, Beijing, China, 2014.